Specific mass shift of the $(4s\,4p)\ ^{1,3}P$ states in calcium studied with many-body perturbation theory

Eva Lindroth, Ann-Marie Mårtensson-Pendrill, and Sten Salomonson*
Department of Physics, Chalmers University of Technology, S-412 96 Göteborg, Sweden
(Received 25 June 1984)

Many-body perturbation theory was applied to calculate the specific mass shift of the $(4s\,4p)\ ^{1,3}P$ states in Ca relative to the $4s$ ground state of Ca^+. The interaction between each valence electron and the core was treated in the same way as the level isotope shifts in the alkali metals in earlier work. The strong correlation between the two valence electrons in neutral Ca was treated self-consistently by iterative solution of the pair equation describing their interaction and its effect on the specific mass shift was evaluated in the same way as for helium. However, also the correlation between the pair of valence electrons and the core is important. All second-order and a large number of third- (and higher-) order diagrams of this type were included, but certain important third-order diagrams could not yet be evaluated. Our final results, -31 and -1533 MHz, respectively, for the $4\,^1P$ and $4\,^3P$ states between ^{48}Ca and ^{40}Ca, show only a qualitative agreement with the experimental values, $-120(9)$ and $-1116(8)$ MHz. This is not surprising, in view of the many competing effects with contributions larger than the final value. The remaining discrepancies are consistent with the expected size of the neglected diagrams and illustrate the importance of the core-valence correlation.

I. INTRODUCTION

Calcium is the only element having two naturally abundant isotopes with doubly magic nuclei. Between these two isotopes, ^{40}Ca and ^{48}Ca, the $f_{7/2}$ neutron shell is filled successively and it has been found[1] that the nuclear charge radii exhibit a certain degree of symmetry around the half-filled $f_{7/2}$ shell (i.e., ^{44}Ca). In particular, since ^{40}Ca and ^{48}Ca have essentially the same charge radii,[1] there is negligible "volume" or "field" shift between them. The "specific mass shift," which is due to a correlation of the electronic momenta through the motion of the nucleus, can thus easily be extracted from optical isotope shift data.

Recent years have seen a vigorous experimental activity in the studies of the isotope shifts in the alkaline earths.[2–10] Systematic measurements of the isotope shifts in transitions to series of excited states have made possible the extraction of level isotope shifts with respect to the ionization limit for the alkaline earths[2,3] in essentially the same way as for the alkali metals,[11–14] although correlation effects between the two valence electrons are evident in both low-lying and highly excited states and complicate the spectral analysis. This strong correlation between the valence electrons leads to complications also in the *ab initio* treatments of properties of the alkaline-earth elements. If perturbation theory is applied it is necessary to treat the interaction between the valence electrons to high orders. Salomonson has recently performed an extensive calculation of the hyperfine structure in the $4s\,4p\ ^{1,3}P$ and $4s\,3d\ ^{1,3}D$ states in ^{43}Ca.[15] The pair correlation between the valence electrons was then treated self-consistently using iterative solution[16] of the pair equation. In addition, important core-valence correlation effects were included by modifying the valence orbitals to approximate Brueckner orbitals.[17] In the present work the specific mass shift of the $4s\,4p\ ^{1,3}P$ states in Ca is calculated using the pair functions obtained by Salomonson[15] to evaluate all second and a large number of third- and higher-order contributions. Many new diagrams, which describe the interaction between the pair of valence electrons and the core, appear in addition to the diagrams evaluated for the alkali metals[18,19] and for He.[20] In Sec. II the diagrams are presented together with the numerical results obtained for the $4s\,4p\ ^{1,3}P$ states in Ca. Section II A gives the results for Ca^+ and a comparison with earlier results for the isoelectronic system K and also with experimental data. The correlation between the valence electrons is discussed in Sec. II B and its effect on the specific mass shift is presented in Sec. II C. The results are summarized in Sec. II D and compared with experimental results as well as with results from other calculations.

II. EVALUATION OF THE SPECIFIC MASS SHIFT

The level isotope shift of the $4s\,4p\ ^{1,3}P$ states in Ca with respect to the doubly ionized inert-gas-like system Ca^{2+} can be illustrated diagrammatically as in Fig. 1, where the box includes one interaction line corresponding to the specific-mass-shift (SMS) operator[18]

$$h^{\mathrm{SMS}}=\sum_{\substack{i\neq j\\ i,j}}\vec{p}_i\cdot\vec{p}_j/2(M+m)$$

(M and m are the masses of the nucleus and the electron, respectively) and an arbitrary number of interaction lines corresponding to the electrostatic repulsion $1/r_{12}$ between the electrons. Experimentally it has so far been possible

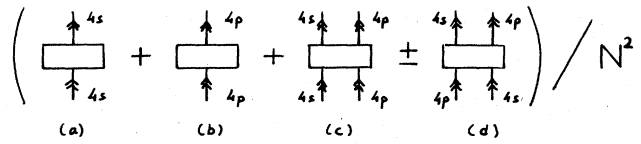

FIG. 1. Schematic illustration of the types of diagrams contributing to the specific mass shift of the $4s4p$ states in Ca with respect to the inert-gas-like core of Ca^{2+}. The norm of the wave function for the valence electrons, which enters due to the use of intermediate normalization, is illustrated in Fig. 2.

to obtain the level shifts only with respect to the alkali-metal-like system, Ca^+.[2] This shift can be evaluated by subtracting from the expression given in Fig. 1 the level isotope shift of the $4s$ ground state of Ca^+ with respect to the inert-gas-like system Ca^{2+}, given by Fig. 1(a), which represents the interaction between the $4s$ electron and the core. [Similarly, diagram 1(b) represents the level isotope shift of the $4p$ state in Ca^+.] It should be noted that due to the normalization correction (given in Fig. 2) which enters in the expression for the shifts in neutral Ca, the cancellation between the $4s$ one-electron contributions to Ca and Ca^+ is not complete and it is thus necessary to evaluate Fig. 1(a). The third and fourth diagrams in Fig. 1 describe the effective direct and exchange interaction between the valence electrons including their interaction, as a pair, with the electron core. Parameters corresponding to the diagrams in Fig. 1 have been used in the analysis of experimental data for Sr (Ref. 4) and Ba.[21]

A. The level shifts in Ca^+

The one-body diagrams, Figs. 1(a) and 1(b), which correspond to the level shifts of the $4s$ [Fig. 1(a)] and $4p$ [Fig. 1(b)] states in Ca^+ with respect to Ca^{2+}, were evaluated in the same way as the level isotope shifts in the alkali-metals[18,19] including all contributions up to second order (Fig. 3). The diagram in Fig. 3(a) is the core-valence part, $-\sum_a^{\text{core}}\langle Oa\,|\,\vec{P}_1\cdot\vec{P}_2\,|\,aO\rangle/(M+m)$, of the expectation value of h^{SMS}. It contributes -1078 MHz for the $4s$ state and -595 MHz for the $4p$ state to the shift between ^{42}Ca and ^{40}Ca. For a scalar operator like h^{SMS} terms involving only core electrons also contribute to the expectation value. However, when the isotope shift with respect to the ionization limit is considered, only the change in the core-core contribution induced by the valence electron is relevant. This change is represented by the diagrams in

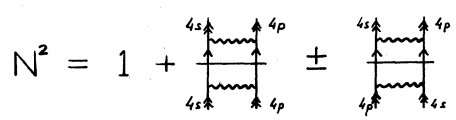

FIG. 2. Diagrammatic representation of the square of the norm of the valence wave function. The positive (negative) sign for the exchange contribution is used for the singlet (triplet) state. Wavy line represents a pair function describing the correlation between the pair of valence electrons.

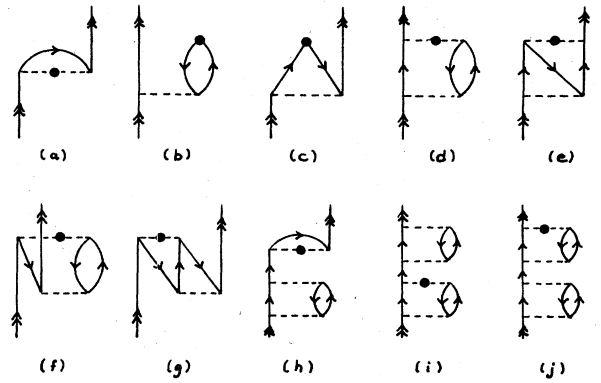

FIG. 3. Contributions to the level shifts in an alkali-metal-like system. Dashed line with (without) a dot represents the specific mass shift (electrostatic) interaction, and the dot in (b) and (c) represents the "effective" SMS operator given in Fig. 4. A line with double arrows is used to denote a valence electron and a down- (up-) going line, with one arrow denoting a core (excited) orbital. The first-order diagram in (a) is the core-valence part of the expectation value of h^{SMS}, (b) and (c) describe a "screening" of the SMS interaction due to the core electrons, (d) and (e) are due to a correlation between the core and the valence electron, and (f) and (g) describe the correlation between two core orbitals. (i)—(j) are examples of diagrams implicitly included when Brueckner orbitals (Fig. 5) are used in the evaluation.

Figs. 3(b) and 3(c), as discussed in Refs. 18 and 19. The effective one-particle SMS operator used in these diagrams is defined in Fig. 4. Obviously, certain higher-order diagrams are included in the "second-order" diagrams 3(b) and 3(c) when the SMS operator from Fig. 4 is used. In hyperfine-structure calculations, diagrams analogous to 3(b) and 3(c) are referred to as "core polarization."[22] However, for a scalar operator they do not describe a real polarization of the core, but only a modification of the radial parts of the orbitals, which is the same for all m_t and m_s states. They could also be considered as a "screening" of the SMS interaction, in analogy with the terminology used for the field shift. We have here used both terms to refer to these diagrams, which lead to a reduction of the SMS by about 40%, as seen from Table I, where the values are given in atomic units. The results in MHz are obtained from these results by using the electron mass $m_e=5.485\,80\times10^{-4}$ amu and the nuclear masses 41.947 650 2 amu and 39.951 619 1 amu for ^{42}Ca and ^{40}Ca, deduced from the atomic masses given in Wapstra and Bos[23] to evaluate the conversion factor $m_e(M_{42}-M_{40})/[(M_{40}+m_e)M_{42}]=4298.97$ MHz/a.u.

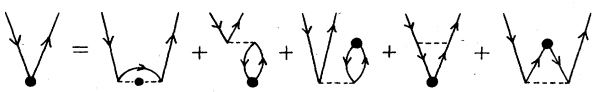

FIG. 4. Diagrammatic illustration of the effective SMS one-body operator.

TABLE I. Results for the level shifts of the $4s$ and $4p$ states in Ca^+ with respect to Ca^{2+} (10^{-2} a.u.).

	$4s$		$4p$	
	HF orbitals	Brueckner orbitals	HF orbitals	Brueckner orbitals
First order [Fig. 3(a)]	−25.0779	−28.8198	−13.8420	−16.7191
All-order screening [Figs. 3(b) and 3(c)]	11.6324	13.6215	5.7289	6.8287
Core-valence correlation [Figs. 3(d) and 3(e)]	5.3077	5.7551	2.9957	3.3152
Core-core correlation [Figs. 3(f) and (3g)]	2.6417	2.8803	0.4799	0.5495
Total	−5.4961	−6.5629	−4.6375	−6.0257

It is well known[24] that inclusion of only single-particle effects [diagrams 3(a)—3(c)] is not sufficient to obtain results close to experimental data, not even for alkali-metal-like systems. For the SMS operator, correlation effects enter already in second order as shown in Figs. 3(d)—3(g). Inclusion of these diagrams leads to the level shift −236 MHz for the $4s$ state and −199 MHz for the $4p$ state between ^{42}Ca and ^{40}Ca.

The results for the level isotope shifts in Ca^+ can be compared to those obtained in K.[18] The larger nuclear charge, which pulls the valence electron further in, leads to larger momenta and a larger overlap between the valence electron and the core. Consequently, the expectation value of $\vec{p}_1 \cdot \vec{p}_2$ is increased. For the $4s$ state all contributions shown in Table I are about twice the size of the corresponding contributions in K although small changes in the degree of cancellation leaves the final result 4 times larger. For the $4p$ state the first-order contribution is about 4 times larger than in K, but the remaining terms, which involve changes in the core orbitals, are changed by different amounts. Most of the contributions from the individual pair excitations are 2—4 times those in K and the total core-core correlation effect is very small for both systems. The total result for the $4s$ state is about 7 times the value for K, leading to a shift of nearly the same size as the $4s$ shift and thus a large cancellation between these two values when the transition shift, −39 MHz, is evaluated.

It was found in connection with hyperfine-structure calculations[17] that important higher-order correlation effects could be included by modifying the orbitals to approximate Brueckner orbitals (Fig. 5). A drastic improvement has been obtained also in a SMS calculation for the $4d$ state in K by using approximate Brueckner orbitals.[25] When the HF orbitals are replaced by the Brueckner orbitals a number of higher-order correlation diagrams are implicitly included. For example, the first-order diagram of Fig. 3(a) will include the third-order diagram 3(h) and the second-order diagram 3(d) will include the fourth-order diagrams 3(i) and 3(j) (and even higher-order terms). The corrections in Fig. 5, which modify the HF orbital to an approximate Brueckner orbital, make the core aware of the presence of the valence electron, which adjusts to the new electron core. This leads to a small expansion of the core and a corresponding contraction of the valence electron. This tends to increase the SMS, which is sensitive to the wave function close to the nucleus. As seen from Table I, the use of Brueckner orbitals increased the size of the SMS by about 20% to −282 MHz for the $4s$ state and by about 30% to −259 MHz for the $4p$ state.

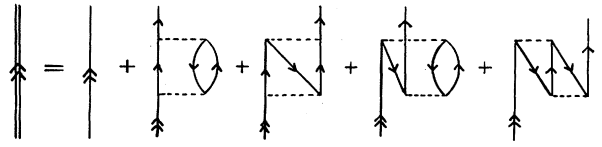

FIG. 5. Diagrammatic illustration of the modification of a valence orbital to an approximate Brueckner orbital.

1. *Comparison with experimental results of Ca^+*

To our knowledge there are no experimental results for the level shifts in Ca^+ and only few measurements have been made on the $4s \rightarrow 4p$ transition shift. Fifteen years ago the isotope shifts of the resonance line in the even isotopes 40, 42, 44, and 48 were measured by Bruch *et al.*[26] and combined with muonic data in a King plot[27,28] in order to estimate the relative importance of mass and field shifts. In a table, they give the result $^{42:40}\Delta\nu^{\mathrm{SMS}} = -24$ MHz, which agrees very well with our result, −23 MHz. However, this good agreement is only accidental. The use of the proper nuclear masses[23] rather than the approximation $M_A = Am_p$ (Ref. 28) in the evaluation of the normal mass shift leads to the experimental value −29 MHz for the SMS.

The result by Bruch *et al.*[26] obtained from the King plot can also be expressed as a SMS constant, −24(10) GHz amu. This value has been somewhat modified by Palmer *et al.*[9] in a recent analysis of available experimental data for Ca where the results by Bruch *et al.* were included in a multidimensional King plot. Palmer *et al.* obtain the estimate −34(12) GHz amu for the SMS constant in the $4s \rightarrow 4p$ transition. In any case, our value, −19 GHz amu, appears to be too small. However, this is

not surprising since we have still neglected a large number of third- (and higher-) order diagrams, which cannot *a priori* be expected to be negligible.

B. The interaction between the two valence electrons in Ca

The two valence electrons in an alkaline-earth element interact strongly with each other. Our initial description of the $4s4p$ states in Ca, where the wave functions for the two valence electrons are created in the potential from the Ca^{2+} core, but do not feel each other, is thus not a very good starting point. As a first step to improve the wave function the correlation between the valence electrons is treated to self-consistency, in analogy with the calculations for He.[20] This can be represented in diagrammatic form by Figs. 6(a)—6(d). About 30 iterations were needed in order to obtain a self-consistent solution. As a second step Brueckner orbitals[17] (Fig. 5) for the valence electrons were used in the evaluation of the valence-valence pair functions. In this way important correlation effects between each valence electron and the core [e.g., Fig. 6(e)] are included in the calculation. As a third step also pair functions describing the core-valence [Fig. 6(f), e.g.] and core-core [Fig. 6(g)] correlation were included on the right-hand side of the valence-valence pair equation. All pair functions were obtained in three logarithmic grids with 59, 69, and 79 points, respectively, in the range $\exp(-7.1)$ to $\exp(4.1)$. More details on the wave function used in the present work are given by Salomonson.[15]

It is often convenient to use "intermediate normalization" in perturbation theory.[29] The initial HF description of the valence pair is then normalized and the pair functions are added, leaving the total function unnormalized. After the third step described above, the norm of the 4^1P state was 1.23 and of the 4^3P state 1.05.[15] If we were staying strictly to the formalism described by Lindgren and Morrison[29] and treating the SMS operator together with the electrostatic interaction in the perturbation expansion and in the pair equation, the lack of normalization would cause no problem. Although this is feasible, the computer programs to implement this scheme have not yet been developed. Instead we use the unnormalized wave function for the valence pair to evaluate the expectation value of h^{SMS} and divide the total result by the square of the norm as indicated in Fig. 1. Of course, the normalization is taken into account also in the pure perturbation expansion. For example, the lowest-order normalization correction to the first-order one-particle diagram [Fig. 3(a)] is given by the "backward" diagram in Fig. 7(a). Similarly, the diagram in Fig. 7(b) describes a normalization correction to the first-order two-body diagram shown in Fig. 8(a). It can be noted that the diagram 7(a) is a two-body diagram and that in the pure perturbation expansion the shift of the $4s4p$ states with respect to the $4s$ state in Ca^+ does not include the $4s$ one-body diagram [except as a part of two-body diagrams analogous to that shown in Fig. 7(a)].

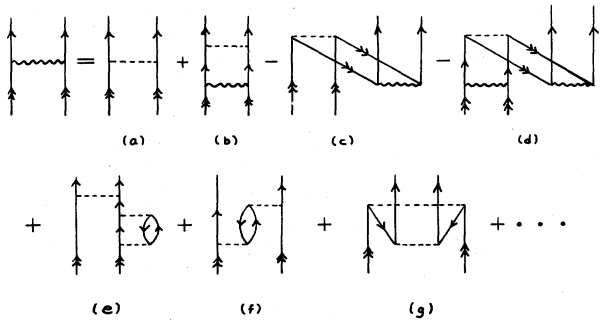

FIG. 6. The valence-valence pair function. (a)—(d) describe the correlation among the valence electrons, (e)—(f) include core-valence correlations and (g) core-core correlation effects.

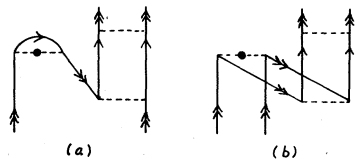

FIG. 7. Example of "backward" diagrams taken into account when (a) the first-order one-body contribution [Fig. 3(a)] and (b) the first-order two-body contribution [Fig. 8(a)] are divided by the lowest-order normalization integrals.

C. Two-body contributions to the specific mass shift

1. *The valence-valence correlation*

The first-, "second"- and "third"-order two-body diagrams involving only valence-valence pair functions are shown in Fig. 8. As discussed in Sec. II B, each diagram includes implicitly a number of higher-order diagrams

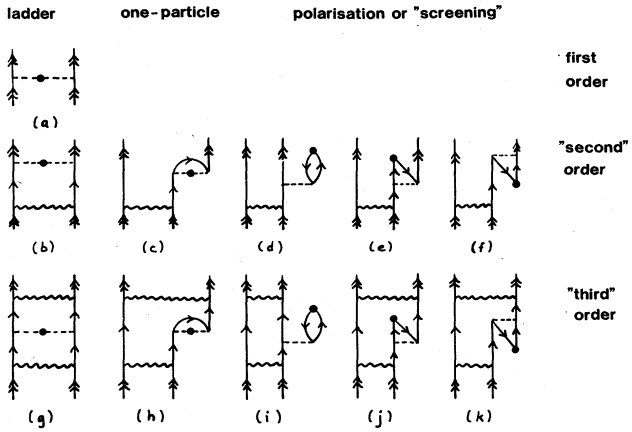

FIG. 8. Valence-valence contributions to the specific mass shift. (a) is the valence-valence part of the expectation value of h^{SMS}. The second- [(b)—(f)] and third- [(g)—(k)] order diagrams, which involve one or two valence-valence pair functions (shown in Fig. 6) include implicitly also higher-order effects. Diagrams analogous to (d) and (i), where the effective SMS interaction is below the electrostatic interaction, have not been shown explicitly but are included in the calculations.

when Brueckner orbitals and iterated pair functions are used.

The first-order two-body diagram, 8(a), is the valence-valence contribution, $-\langle 4s\,4p \mid \vec{p}_1\cdot\vec{p}_2 \mid 4p\,4s\rangle/(M+m_e)$, to the expectation value of h^{SMS}. Only the exchange term enters since the momentum operator $\vec{p}$ is an odd-parity operator with rank 1. These properties also restrict the possible pair excitations in the second-order "ladder" diagram, 8(b), to $4s\,4p \rightarrow ps,pd$ and $4s\,4p \rightarrow sp,dp$, respectively, for the direct and exchange two-body contributions. Thus, in the *pd* limit, all excitations contributing to true second-order diagrams are included, whereas in the *sp* limit several of them are missing. It is then not very surprising that there is a rather large change in the results when the *pd* excitations are included and that the inclusion of *df* excitations is less important, as shown in Table II, where the sum of contributions from the diagrams in Fig. 8 evaluated in different angular limits and with different types of valence-valence pair functions are given.

The results in Table II are presented as the contributions to the singlet and triplet states. As discussed above, these are obtained by adding (subtracting) the exchange contribution to (from) the direct contribution and then dividing the result by the appropriate normalization correction. The use of Brueckner orbitals is even more important here than for the one-body contributions (Sec. II A). For example, the contribution to the singlet state is doubled when Brueckner orbitals are used, showing that the correlation between each valence electron and the core has a large influence also on the correlation between the valence electrons. Most of the correlation between the core and the valence electrons is, indeed, taken into account by modifying the valence orbitals; the inclusion of the core-core and core-valence diagrams [Figs. 6(f) and 6(g)] on the right-hand side of the valence-valence pair equation gives only minor contributions, as seen from the last two lines of Table II.

Table III gives the contributions from different groups of diagrams in Fig. 8 evaluated with *pd*-limit pair functions based on Brueckner valence orbitals. It is somewhat surprising that the SMS interaction between the valence pair and the core electrons ["one-particle," 8(c) and 8(h) and "polarization," 8(d)—8(f) and 8(i)—8(k) diagrams] is even more important than the SMS interaction between the two correlated valence electrons themselves [Figs. 8(b) and 8(g)]. Possibly this can be ascribed to the large momenta of the core electrons.

TABLE II. Results for the valence-valence correlation diagrams in Fig. 8 evaluated in different angular limits (10^{-2} a.u.).

	$4s\,4p$ (^1P)	$4s\,4p$ (^3P)
Correlated valence pair in the HF potential from the Ca^{2+} core		
sp limit	1.7063	−0.2662
pd limit	3.4407	0.5040
df limit	3.5159	0.4538
With Brueckner orbitals		
pd limit	7.4924	2.1336
With lowest-order valence-core and core-core correlation and Brueckner orbitals		
pd limit	7.9790	2.6771
df limit	8.0717	2.6103

TABLE III. The contributions from the different diagrams in Fig. 8 to the *pd* limit when Brueckner orbitals are used. The values for the individual diagrams are calculated in a 59-point grid only, whereas the extrapolated results are based on three grids. Given after the order of the contributions are the corresponding figure numbers (10^{-1} a.u.).

	Direct	Exchange
Ladder diagrams		
First order, 8(a)[a]		5.9475
Second order, 8(b)	3.9373	0.0069
Third order, 8(g)	−1.1706	0.0397
One-particle diagrams		
Second order, 8(c)	16.3306	1.6224
Third order, 8(h)	−9.9695	−6.2043
Polarization diagrams		
Second order, 8(d),8(e),8(f)	−7.2957	−0.5611
Third order, 8(i),8(j),8(k)	4.2625	2.5970
Total	6.0950	3.4481
Extrapolated	5.9173	3.6839

[a]The HF result for the valence-valence expectation value [Fig. 8(a)] is 5.3891×10^{-2} and the extrapolated result with Brueckner orbitals is 5.9221×10^{-2}.

The polarization diagrams 8(d)—8(f) and 8(i)—8(k) were calculated using single-particle functions containing the screening of the SMS operator by the core electrons (Fig. 4), as discussed in Sec. II A, which were used to evaluate also the "all-order screening" contributions to the level shifts of Ca^+.

As seen from Table III, there is a large cancellation between the different diagrams. For example, of the large second-order one-particle contribution, 8(c), to the direct part, 16×10^{-2} (atomic units are used unless otherwise stated), only 3×10^{-2} remains after addition of the "polarization" diagrams 8(d)—8(f) and 8(i)—8(k) and the "third-order one-particle" contribution 8(h). This cancellation makes the result quite sensitive to small changes in the wave function and is one reason for the drastic changes when the HF orbitals are replaced by Brueckner orbitals in the calculation of the pair functions (Table II). When HF orbitals are used to obtain the pair functions, the second-order diagrams 8(b)—8(f) give a positive contribution of 7.95×10^{-2} to the singlet state, while the third-order diagrams 8(g)—8(k) give a somewhat larger negative contribution, -8.31×10^{-2}. The use of Brueckner orbitals increases the positive contributions to 10.28×10^{-2} and reduces the negative contribution to -7.4×10^{-2}. The sum of these terms thus raises from -0.4×10^{-2} to $+3.0\times10^{-2}$.

2. The core-valence correlation

Although a large number of diagrams are shown in Fig. 8 and many important core-valence correlation effects are included in the valence orbitals and pair functions, there are diagrams already in second order not yet included. These are shown in Figs. 9(a)—9(f). Figures 9(g)—9(i) show some similar third-order diagrams.

The diagrams in Figs. 9(a)—9(d) contain one core-valence pair function and describe how the SMS interaction between the core and one valence electron is screened by the other valence electron. There are two types of contributions to each diagram, one where the core-valence pair functions contains the $4s$ electron and one where it contains the $4p$ electron. Diagrams 9(b)—9(d) were found to be rather small, as seen from Table IV, which shows the contributions from pair functions describing the $4s$-core correlation. Diagram 9(a) contributes only to the exchange part due to the angular restrictions of h^{SMS}. It is about 10 times larger than diagrams 9(b)—9(d), in spite of large cancellations; the $4s$ part contributes 4.1504×10^{-2} and the $4p$ part -4.7561×10^{-2} to diagram 9(a).

Diagram 9(f) describes the SMS interaction between the valence pair and a pair of core electrons and is evaluated using one core-core pair function. The corresponding third-order diagram 9(i) needs also a valence-valence pair function in the evaluation. As seen from Table V, these core-core correlation diagrams are much smaller than the core-valence correlation diagrams.

Of the third-order diagrams analogous to the second-order diagrams, 9(a)—9(e), only those in Figs. 9(g) and 9(h), corresponding to diagrams 9(a) and 9(c), were included. They were evaluated using one core-valence and one iterated valence-valence pair function. As seen from Table IV, they are about 5 times smaller than their second-order counterparts 9(a) and 9(c) [except for the direct contribution where 9(a) and 9(c) do not contribute due to angular restrictions]. The contribution from 9(g) is significant, whereas that from 9(h) is very small. Since diagrams 9(b) and 9(d) are of the same size as 9(c), we assume that their corresponding third-order contributions are very small, just as 9(h) was found to be.

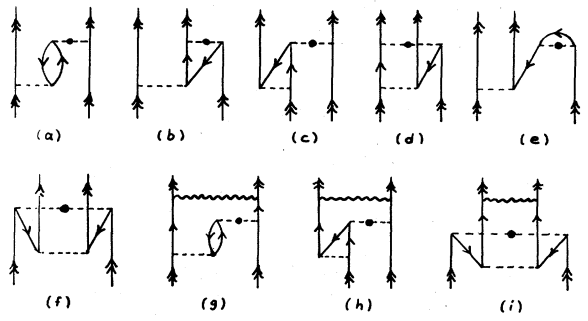

FIG. 9. Core-valence [(a)—(d) and (g)—(h)] and core-core [(f) and (i)] correlation diagrams contributing to the two-body SMS parameters. Of the third-order diagrams analogous to the second-order diagrams (a)—(f) only those shown in (g)—(i) have been evaluated.

TABLE IV. Contributions from the $4s$-core correlation to the different diagrams in Fig. 9. The individual values are given for a 59-point grid. Thus the total "second"- and "third"-order results differ somewhat from the extrapolated values given in Table V (10^{-2} a.u.).

	Direct	Exchange
Second order		
Fig. 9(a)		4.1504
Fig. 9(b)	−0.0240	0.0073
Fig. 9(c)		0.0123
Fig. 9(d)	−0.0084	0.0332
Fig. 9(e)	−0.3736	0.4823
Total second order	−0.4060	4.6855
Third order		
Fig. 9(g)	−1.1875	0.7942
Fig. 9(h)	−0.0095	0.0012
Total third order	−1.1969	0.7954

Diagram 9(e) was evaluated using a valence single-particle function containing the "effective one-body SMS interaction" (Fig. 4). However, no orthogonality was enforced to the core and the overlap with the core orbitals was used in the evaluation of diagram 9(e). At present, we are not able to calculate the third-order diagrams corresponding to 9(e), but in view of the relative smallness of 9(e), we do not expect very large contributions from this neglected diagram. Table V gives a summary of the results obtained for the diagrams in Fig. 9.

3. SMS corrections to Brueckner orbitals

The diagrams in Figs. 10(a)—10(d) contain a part analogous to the approximate Brueckner valence orbital shown in Fig. 5, with the upper electrostatic interaction replaced by a SMS interaction. However, instead of obtaining such "SMS Brueckner orbitals," we evaluated them using one iterated pair function and one core-valence [Figs. 10(a) and 10(b)] or core-core [Figs. 10(c) and 10(d)] pair function. Diagram 10(e) is very similar to diagram 10(a)—only the SMS interaction and the first electrostatic interaction are interchanged. Also this diagram contains a

TABLE V. Summary of the contributions from the core-valence correlation diagrams in Fig. 9 (10^{-2} a.u.).

	Direct	Exchange
Second order Figs. 9(a)—9(f):		
core-valence correlation with $4s$	−0.3846	4.5324
core-valence correlation with $4p$	−0.0616	−3.3779
core-core correlation [Fig. 9(f)]	0.0067	0.0181
Third order Figs. 9(g)—9(i):		
core-valence correlation with $4s$	−1.1598	0.6818
core-valence correlation with $4p$	−0.8986	−0.5339
core-core correlation [Fig. 9(i)]	−0.0018	−0.0050
Total	−2.4997	1.3155

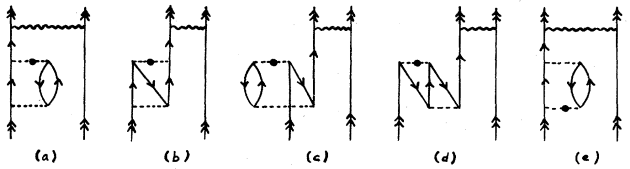

FIG. 10. Diagrams containing a part which can be considered as a SMS contribution to a Brueckner orbital (Fig. 5).

part which could be considered as a contribution to a SMS Brueckner orbital. However, to evaluate this diagram we would need a pair function involving the SMS operator itself and we have not yet implemented the computer programs to obtain such pair functions.

Diagrams 10(a) and 10(b) were found to be very important (Table VI). The contribution to the triplet state, e.g., was larger than the contributions from the ladder, one-particle, and polarization diagrams in Fig. 8. Since these diagrams were found to be so important, we expect important contributions also from diagrams like 10(e). These probably account for a large part of the remaining discrepancy between our final results and the experimental values (Table VII).

D. Summary and discussion of the results

A summary of the contributions obtained from different groups of diagrams included in the present work is shown in Table VII, together with the experimental results for the level shifts with respect to the ground state of Ca^+. Only the values obtained with the best orbitals and pair functions available are given.

The valence-valence correlation diagrams in Fig. 8 are important for both states considered, but in particular for the singlet state. This is consistent with the observation that there is a larger admixture of excited states in the singlet state (the normalization integral is 1.23 compared to 1.05 for the triplet state). The diagrams in Fig. 9, which include core-core and core-valence correlation effects, are much more important for the triplet state. This

TABLE VI. Contributions due to SMS modification of Brueckner orbitals (Fig. 10). The individual values are given from a calculation in 79-point grid, but the total value is calculated in three grids and extrapolated (10^{-2} a.u.).

	Direct	Exchange
Core-valence correlation with $4s$ [Figs. 10(a) and 10(b)]	−1.7796	0.3594
Core-valence correlation with $4p$ [Figs. 10(a) and 10(b)]	−2.1788	−0.6674
Core-core correlation [Figs. 10(c) and 10(d)]	−0.4680	0.0102
Total	−4.4264	−0.2978
Extrapolated	−4.2023	−0.3020

is due to a certain cancellation between a negative direct contribution and a positive exchange contribution of about the same magnitude (Table V). The modification of the valence orbitals to SMS-Brueckner orbitals (Fig. 10) is of similar importance for both states since, as seen from Table VI, the direct contribution is more than 10 times larger than the exchange contribution. A large part of the diagrams in Fig. 10 can probably be described as a potential correction on one valence electron due to the presence of the other and would be included in the "one-body" diagrams shown in Fig. 2 if another potential was used for the valence orbitals.

There is a large cancellation between different groups of diagrams, but also within the groups (as seen from Table II, e.g.). For the 4^1P state, certain individual contributions are up to 50 times as large as the final result. In view of these cancellations it is not surprising that a discrepancy remains between our final results, -0.21×10^{-2} and -10.81×10^{-2}, respectively for the singlet and triplet state, and the corresponding experimental values, $-0.80(6)\times10^{-2}$ and $-7.41(5)\times10^{-2}$. [These values are obtained from the level shifts −120(9) MHz and −1116(8) MHz between ^{48}Ca and ^{40}Ca, given in Ref.

TABLE VII. Summary of contributions to the level isotope shift constant K^{SMS} for the $(4s4p)\ ^1P$ and ^3P states in Ca relative to the $4s$ ground state of the ion Ca^+ (10^{-2} a.u.).

	$(4s4p)^1P$	$(4s4p)^3P$
Fig. 8, valence-valence correlation	8.0717	2.6103
Fig. 9, core-valence and core-core correlation	−0.9615	−3.6373
Fig. 10, SMS modifications of Brueckner orbitals	−3.6573	−3.7185
Fig. 3, one-body contribution from $4p$	−4.8926	−5.7448
Fig. 3, contribution from $4s$ due to the normalization correction	1.2341	0.3060
Total[a]	−0.2056	−10.1843
Experiment[a]	−0.80(6)	−7.41(5)

[a]For the shift between ^{48}Ca and ^{40}Ca, the conversion factor 15057 MHz/a.u., gives the theoretical values −31 and −1533 MHz, respectively, for the singlet and triplet state, which can be compared to the experimental results −120(9) MHz and −1116(8) MHz (Ref. 2).

2.] Since the diagram in Fig. 10(a) is so important, a large part of the discrepancy can probably be ascribed to neglected diagrams of the type in Fig. 10(e). The evaluation of the one-body contributions (Fig. 3) may be another cause of the discrepancy. No attempt has yet been made to include systematically the third-order contributions to the level shifts in Ca^+ and we know that our value for the $4s \rightarrow 4p$ transition shift is somewhat smaller than the experimental value (Sec. II A). However, we have no information about the error in each level shift. It may seem surprising, but, since we know exactly which diagrams correspond to the level shifts in Ca^+, experimental values for these level shifts, if available, could be used instead of our second-order results to obtain better values for the level shifts in neutral Ca.

E. Comparison with other work

The first *ab initio* calculation of the SMS in Ca was performed by Bauche.[24] In separate Hartree-Fock (HF) calculations for the singlet and triplet states ("*LS*-dependent HF") he obtained the shifts -130.1565 a.u. for the singlet state and -130.2561 a.u. for the triplet state with respect to the fully ionized system. The difference, -0.0996, is very similar to the difference between our final results in spite of our inclusion of a large number of correlation effects. In order to compare also the level shifts with respect to the $4s$ ground state of Ca^+ we need the HF value for the total shift in the $4s$ state. This can be obtained by adding to the HF value, -130.0448, for the core-core contribution the sum of the "first-order core-valence" and screening effects for the $4s$ state, given in the first column of Table I. The total shift -130.1792, for the $4s$ state in Ca^+ is then subtracted from the HF values for the shifts of the singlet and triplet states, giving the results shown in Table VIII. The value for the triplet state agrees well with the experimental result, whereas for the strongly perturbed singlet state the wrong sign is obtained.

Due to our somewhat unphysical starting potential from the inert-gas-like core of Ca^{2+}, a large part of the effects classified as "valence-valence" correlation (Fig. 8) are taken into account in a complete HF calculation. For comparison, we give in Table VIII the *sp*-limit value obtained when all correlation effects with the core are neglected (and using the norm obtained in the *sp* limit[15]). These values are quite similar to the HF values, particularly for the triplet state. The differences are due to our admixture of higher excited *sp* states. The inclusion of excited *pd* configurations (which enter already in second order) was found to give important contributions as well. By including such configurations in a multiconfigurational Hartree-Fock (MCHF) calculation, e.g., it would be possible to include a large part of the diagrams in Fig. 8 to the *pd* limit, but again no correlation with the core would be accounted for. The *pd*-limit results neglecting the core-valence correlation are given in the third row of Table VIII. A MCHF calculation including valence-valence correlation was performed by Bauche and coworkers for the field shift in Ca (Ref. 30) and for both field and mass shift in Sr.[10] At this level the difference between the singlet and triplet states is quite well reproduced, but the singlet state still has the wrong sign.

Recently, Chambaud *et al.*[31] attempted to go beyond the HF level using the CIPSI method (configuration interaction by perturbation of a multiconfiguration wave function selected iteratively, Ref. 32). They found very large correlation contributions, about -13 a.u., not observed in the present work. However, most of this effect is the same for all the states considered ($4s^2$, $4s\,4p$, $4s\,3d$, and $4s\,5s$)—the variation between the states is at most 0.2 a.u. This enormous contribution obtained when the correlation with the core is included is most likely due to closed diagrams, which describe the correlation among the

TABLE VIII. Comparison between theoretical and experimental results for the $4s\,4p\ ^{1,3}P$ states in Ca (10^{-2} a.u.).

	^1P	^3P	$(^3P-{}^1P)$
LS-dependent HF[a]	2.27	−7.69	−9.96
HF + valence-valence correlation (Fig. 8)			
sp limit[b]	1.925	−7.392	−9.32
pd limit[b]	1.452	−6.155	−7.61
Brueckner orbitals + total correlation [Figs. 3, 8, 9, and 10(a)–10(f)][b]	−0.206	−10.184	−9.98
Experiment	−0.80(6)[c,d]	−7.41(5)[c,e]	−6.61(2)[d,e] −6.59(1)[f,e] −6.604(12)[g]

[a]Bauche, Ref. 24.
[b]This work.
[c]Lorenzen *et al.*, Ref. 2.
[d]Brandt *et al.*, Ref. 5.
[e]Bergmann *et al.*, Ref. 7.
[f]Andl *et al.*, Ref. 6.
[g]Palmer *et al.*, Ref. 9.

core electrons. These enter the shifts of Ca^{2+} with respect to the fully ionized system, but cannot be observed in optical spectroscopy. Obviously, if these pure core-core correlation effects are included, it is very important to calculate them to the same level of accuracy for all states considered in order to make the cancellation between their contributions complete. The final result by Chambaud *et al.*[31] for the isotope shift between the 4^1P and 4^3P states, -0.14, is actually worse than the HF value, in spite of the inclusion of a large number of correlation effects. The same is true for our result for the triplet state. As we have seen in the preceding sections, there are many competing correlation effects and they all have to be considered very carefully.

III. CONCLUSION

In spite of the need for theoretical calculations of the electronic factors for the specific mass shift and field shift in the interpretation of the results of the extensive experimental studies of isotope shifts, only few attempts have been made to calculate these factors *ab initio*. The specific mass shift, which depends on a coupling between pairs of electronic momenta, is very sensitive to correlation effects and a careful theoretical study is thus needed to obtain sufficiently accurate and reliable values. The correlation between the valence electrons in Ca is very strong and gives large contributions to the specific mass shift. However, as seen from the present work, the correlation between each valence electron and the core cannot be neglected. Although the valence-valence interaction has been treated to all orders, certain third-order core-valence correlation diagrams could not yet be evaluated and only a qualitative agreement with experiment was obtained. We thus conclude that it is necessary to treat also the correlation between the core and the valence electrons more accurately in order to gain a better understanding of the specific mass shift in Ca.

ACKNOWLEDGMENTS

We have benefited from discussing the results of this work with Dr. L. R. Pendrill. Financial support from the Swedish Natural Science Research Council is gratefully acknowledged.

*Present address: Department of Physics, University of Virginia, Charlottesville, VA 22901.

[1]H. D. Wohlfahrt, E. B. Shera, M. V. Hoehn, Y. Yamazaki, and R. M. Steffen, Phys. Rev. C **23**, 533 (1981).
[2]C.-J. Lorenzen, K. Niemax, and L. R. Pendrill, Phys. Rev. A **28**, 2051 (1983).
[3]W. Hogervorst and E. R. Eliel, Z. Phys. A **310**, 19 (1983).
[4]E. R. Eliel, W. Hogervorst, T. Olsson, and L. R. Pendrill, Z. Phys. A **311**, 1 (1983).
[5]H.-W. Brandt, K. Heilig, H. Knöckel, and A. Steudel, Z. Phys. A **288**, 241 (1978).
[6]A. Andl, K. Beck, S. Göring, A. Hanser, G. Nowicki, H. Rebel, G. Schatz, and R. C. Thompson, Phys. Rev. C **26**, 2194 (1982).
[7]E. Bergmann, P. Bopp, C. Dorsch, J. Kowalski, F. Träger, and G. zu Putlitz, Z. Phys. A **294**, 319 (1980).
[8]E. Mattias, H. Rinneberg, R. Beigang, A. Timmermann, J. Neukammer, and K. Lücke, in *Proceedings of the Eighth International Conference on Atomic Physics (ICAP-8), Göteborg, Sweden, August 1982* (Plenum, New York, 1983), p. 543, and references therein.
[9]C. W. P. Palmer, P. E. G. Baird, S. A. Blundell, J. R. Brandenburger, C. J. Foot, D. N. Stacey, and G. K. Woodgate, J. Phys. B **17**, 2197 (1984).
[10]A. Aspect, J. Bauche, A. L. A. Fonseca, P. Grangier, and G. Roger, J. Phys. B **17**, 1761 (1984).
[11]B. P. Stoicheff and E. Weinberger, Can. J. Phys. **57**, 2143 (1979).
[12]S. Liberman and J. Pinard, Phys. Rev. A **20**, 507 (1979).
[13]K. Niemax and L. R. Pendrill, J. Phys. B **13**, L461 (1980); **15**, L147 (1982).
[14]C.-J. Lorenzen and K. Niemax, J. Phys. B **15**, L139 (1982).
[15]S. Salomonson, Z. Phys. A **316**, 135 (1984).
[16]A.-M. Mårtensson, J. Phys. B **12**, 3995 (1979).
[17]I. Lindgren, J. Lindgren, and A.-M. Mårtensson, Z. Phys. A **279**, 113 (1976).
[18]A.-M. Mårtensson and S. Salomonson, J. Phys. B **15**, 2115 (1982).
[19]E. Lindroth and A.-M. Mårtensson-Pendrill, Z. Phys. A **309**, 277 (1983).
[20]E. Lindroth and A.-M. Mårtensson-Pendrill, Z. Phys. A **316**, 265 (1984).
[21]L. R. Pendrill, Z. Phys. A **316**, 275 (1984).
[22]S. Garpman, I. Lindgren, J. Lindgren, and J. Morrison, Phys. Rev. A **11**, 758 (1975); Z. Phys. A **276**, 167 (1976).
[23]A. H. Wapstra and K. Bos, At. Data Nucl. Data Tables **19**, 177 (1977).
[24]J. Bauche, Thèse, Université de Paris (1969); J. Phys. (Paris) **35**, 19 (1974).
[25]S. Hörbäck, L. Pendrill, A.-M. Pendrill, and M. Pettersson, Z. Phys. A (to be published).
[26]R. Bruch, K. Heilig, D. Kaletta, A. Steudel, and D. Wendlandt, J. Phys. (Paris) Colloq. **30-51** (1969).
[27]W. H. King, J. Opt. Soc. Am. **53**, 638 (1963).
[28]K. Heilig and A. Steudel, At. Data Nucl. Data Tables **14**, 613 (1974).
[29]I. Lindgren and J. Morrison, *Atomic Many-Body Theory,* Vol. 13 of *Springer Series in Chemical Physics* (Springer, Berlin, 1982).
[30]A. L. A. Fonseca and J. Bauch, Z. Phys. A **318**, 13 (1984).
[31]G. Chambaud, B. Lévy, and D. N. Stacey, in *Proceedings of the EGAS Conference, Liège, 1982* (unpublished).
[32]B. Huron, J. P. Malrieu, and P. Rancurel, J. Chem. Phys. **58**, 5745 (1973).